Discovery of a small molecule having both potent anti-fibrotic and anti-inflammatory capabilities

Han-Soo Kim,[1,2*] Moon Kee Meang[3*], MinJu Ham[3], Baik L. Seong[4], Ik-Hwan Kim,[5] and Byung-Soo Youn[3#]

[1]Department of Biomedical Sciences, Catholic Kwandong University College of Medical Convergence, Gangneung-si, Gangwon-do 25601, Republic of Korea; [2]Basic Research Division, Biomedical Institute of Mycological Resource, College of Medicine, Catholic Kwandong University, Gangneung-si, Gangwon-do 25601, Republic of Korea; [3]OsteoNeuroGenInc, Seoul, 08501, Republic of Korea; [4]Department of Biotechnology, Yonsei University, Seoul 03722, Republic of Korea; [5]Department of Biotechnology, Korea University, Seoul 02841, Republic of Korea

Running title: Chromone scaffold-based anti-fibrotic and anti-inflammatory therapeutics

*These authors contributed equally to this investigation.

[#]To whom correspondence should be addressed: OsteoNeuroGen, Inc. Ace High-end Tower 9th 233, Gasandigital-1-ro, Geumcheon-gu, Seoul, 08501, Republic of Korea; byung4jc@gmail.com; Tel. +82-2-6267 2737; Fax. +82-2-6267-2740

Abstract

Fibrosis is caused by the proliferation of pathogenic myofibroblasts and the deposition of massive amounts of soluble collagen, altering the homeostasis of extracellular matrix (ECM) biogenesis and resulting in tissue scarring. Because a chromone scaffold (CS)-containing small molecule called eupatilin was shown to curb lung fibrosis, a new CS-containing analog, ONG41008, was generated. Plasma exposure was significantly increased. Orally-administered ONG41008 was more potent than pirfenidone at ameliorating fibrosis in a bleomycin-induced lung fibrosis model (BLM). ONG41008 also completely inhibited the trans-differentiation to myofibroblasts of ONGHEPA1, being a primary hepatic stellate cells (HSC) cell line, and of primary diseased human lung fibroblasts (DHLFs) derived from patients with idiopathic pulmonary fibrosis. ONG41008 inhibited the expression of LTBP1 and LAP, dismantling the latent TGFβ complex, likely limiting binding of TGFβ to TGFβ receptors I and II. ONG41008 also markedly inhibited the phosphorylation of SMAD2 and SMAD3, the induction of NADPH oxidase 4 (NOX4) in both cell types, and the production of reactive oxygen species. ONG41008 also completely inhibited the induction of chemokine ligands 2 (*Ccl2*) and 7 (*Ccl7*) and induced robust autophagy, suggesting that ONG41008 could curb liver inflammation and fibrosis. STAM mice model was orally administered with 50 mg/kg (mpk) ONG41008 exhibited high nonalcoholic fatty liver disease scores, suggesting that ONG41008, together with anti-diabetic drugs like GLP1 and peroxisome proliferator-activated receptor agonists, could reduce the development of nonalcoholic steatohepatitis (NASH).

Treatment of macrophages with ONG41008 and lipopolysaccharide (LPS) markedly inhibited the expression of *TNFα, Interleukin 1β, CHOP, CCL2*, *CCL7*, and *CXCL2*. ONG41008 also efficiently blocked the endocytosis of CD14, a LPS coreceptor, and retained its expression on the plasma membrane, but had no effect on the cellular distribution of MD-2,

TLR4 and Myd88. Taken together, these findings showed that ONG41008 is a bifunctional agent, with both anti-inflammatory and anti-fibrotic activities. This drug may be powerful and safe in the treatment of fibrosis and fibrotic diseases, including NASH, as well as in the treatment of autoimmune, inflammatory, and neuroinflammatory diseases, including rheumatoid arthritis, inflammatory bowel disease, multiple sclerosis, and sepsis.

Introduction

Idiopathic pulmonary fibrosis (IPF) is a rare type of interstitial lung disease (ILD).[1] It is associated with high mortality and morbidity rates, with the median survival of patients with IPF ranging from 3~5 years after diagnosis and most patients dying within 5 years.[2] Nonalcoholic fatty liver disease (NAFLD) is becoming pandemic worldwide due to over-nutrition. Nonalcoholic steatohepatitis (NASH) is an extreme manifestation of NAFLD, associated with various types of immunometabolic dysfunction, including steatosis, lobular inflammation and progressive fibrosis.[3,4] Mitigation of liver fibrosis can inhibit the development of NASH.[5] The development of potent anti-fibrotic and anti-inflammatory agents is of paramount importance in the treatment of IPF and NASH. To date, however, no curative drugs for these conditions have become available.[6,7] Two small-molecule anti-fibrotic drugs, pirfenidone (Esbriet) and nintedanib (Ofev), were recently approved for the treatment IPF,[8] but their efficacies and side effects must be improved to successfully treat these diseases. Moreover, the anti-fibrotic mechanism of action of pirfenidone remains to be determined.

Flavones are members of the polyphenol family, a group of >10,000 compounds predominantly found in the plant kingdom.[9] In general, these phytochemicals protect plants from radiation damage.[10] Due to their anti-oxidant and anti-inflammatory activities, flavones have long been used to treat inflammatory diseases such as arthritis and asthma[11] Chromone, 1,4-benzopyrone-4-one, is a central chemical scaffold for flavones,[12] with chromone scaffold-containing derivatives (CSD) being a diverse family, with branching chemical residues coupled to this core chemical scaffold.[13] We recently reported that eupatilin, a CSD from an *Artemisia* species, dramatically inhibits lipopolysaccharide (LPS)-induced osteoporosis, partially via actin depolymerization[14] and the downregulation of multiple genes associated with the epithelial–mesenchymal transition (EMT). The present study shows that a noble CSD, ONG41008, can block the induction of Type 2 EMT, also called fibrogenesis, arrest cell growth

and alter cell morphology, thereby substantially ameliorating lung fibrosis. Its intrinsic potential that CD14 renders resistant to endocytosis may play a critical role in blocking LPS-induced activation followed by autoreactive-T cells-mediated hyper inflammation.

Results and Discussion

Non-GLP toxicokinetic studies in rats indicated that ONG41008 was present in plasma more than 12 hr after oral administration, resulting in a Tmax of 1–2 hr and a Cmax of 260.8 ± 41.4 ng (Supplementary Figure S1A). The tissue pharmacokinetics (PK) of orally administered ONG41008 in mice and rats over 2 hr were assessed. Oral gavage of ONG41008 for 14 days showed that this agent was non-toxic (data not shown), as was a single non-GLP dose in beagle dogs (Supplementary Figure S1B).

Within 30 min after oral administration, ONG41008 was largely detected in plasma, lungs, liver, and kidneys of mice and rats (Supplementary Figure 2). Treatment of ONGHEPA1 primary (HSCs) line and primary diseased human lung fibroblasts (DHLFs) with transforming growth factor-β (TGFβ) enhanced the expression of α-smooth muscle actinin (αSMA), but these increases were substantially mitigated by treatment with ONG41008 (Figure 1A and 1B). Similarly, TGFβ induced expression of the pharmacodynamic markers C*ollagen11α1*, C*ollagen1α1*, and *Periostin*, but these increases were reduced by ONG41008, suggesting that ONG41008 may act directly on pathogenic myofibroblasts in both lung and liver fibrotic tissues. ONG41008 markedly inhibited the phosphorylation of both SMAD2 and SMAD3, not of ERK, suggesting that phosphorylated SMAD2 and/or SMAD3 may translocate to the nucleus, activating fibrogenesis, a process also called type II epithelial-to-mesenchymal transition (EMT)(Figure 1C). Because eupatilin was able to depolymerize F-actin, we hypothesized that F-actin may be also a substrate for ONG41008. Under control conditions, F-actin stress fibers were localized at cell focal adhesion regions (Figure 1D). Although treatment of ONGHAPA1 cells with ONG41008 resulted in massive actin depolymerization, this depolymerization did not occur in cells stimulated with the anti-IPF drugs pirfenidone and nintedanib, suggesting that these agents have no direct effects on actin in these cells. An *in vitro* actin polymerization/depolymerization assay showed that ONG41008 was a powerful

inhibitor of actin polymerization (Figure 1E) as well as an enhancer of actin depolymerization (Figure 1F). To further assess the mechanism of action (MOA) of ONG41008, DHLFs treated with TGFβ and/or ONG41008 were stained with antibodies recognizing the components of the latent human TGFβ complex. Treatment with TGFβ markedly induced the expression of LTBP1 and LAP1 and their secretion into the extracellular matrix (ECM), whereas LTBP4 was only partially affected or unaffected by ONG41008 (Figure 1G). ONGHEPA1 cells converted to myofibroblasts by treatment with TGFβ for 24 hr and treated with TGFβ and ONG41008 for another 24 hr showed massive downregulation of LTBP1, LAP1, and integrin α5β3 expression, with these molecules confined to endosome-like vesicles, as well as the disappearance of actin stress fibers (Figure 1H). To identify the ONG41008-suppressible fibrosis-inducing genes (FIGS), DHLFs were differentially treated with TGFβ in the presence or absence of ONG41008 and transcriptomic changes were analyzed by RNA-seq analysis, using the selection process illustrated in Figure 2A. While seventy-seven ONG41008-suppressible FIGS with $p>0.005$ were detected in DHLFs (Figure 2B) twenty-five FIGS were detected by ONG21001 (eupatilin) (Supplementary Figure S3), suggesting that, therapeutics per se, ONG41008 is three-fold as high as ONG21001. Many of those genes were previously found to be fibrogenic, including those encoding NOX4, CTGF, PERIOSTIN, LOX, and CDH2.[15-17] Induction of *NOX4*, which encodes NADPH oxidase 4, is associated with the production of reactive oxygen species (ROS) and with several important signaling events, including LPS signaling and inflammasome activation.[18] These findings suggested that NOX4 plays an important role in the pathogenesis of myofibroblasts. Interactome analysis showed that NOX4 was functionally related to endothelin (EDN) 1, connective tissue growth factor (CTGF) and insulin-like growth factor binding protein-3 (IGFBP-3) (Figure 2C). HSCs play a pivotal role in hepatic inflammation as well as liver fibrosis.[19,20]

To assess whether ONG41008 can suppress the induction of *NOX4*, thereby downregulating ROS production, ONGHEPA1 cells were treated with TGFβ, and the induction kinetics of *NOX4* mRNA and protein, along with those of several fibrogenic genes, were analyzed. *Nox4* mRNA and NOX4 polypeptide were significantly induced by TGFβ, with ONG41008 being able to block their induction, suggesting that ONG41008 inhibits the induction of *NOX4* (Figure 3A). Immunocytochemistry (ICC; Figure 3B) and ROS dye staining (Figure 3D) also showed that the production of ROS was significantly attenuated by ONG41008. Similar results were observed in DHLFs (Figure 3C). ONG41008 also blocked the induction of *NOX4*, *CCL2*, and *CCL7* (Figure 3E), suggesting that ONG41008 could modulate the migration of macrophages to the liver.

Autophagy plays a pivotal role in attenuating fibrosis.[21,22] To determine if ONG41008 could induce the induction of autophagosomes, DHLFs and ONGHEPA1 cells were treated with TGFβ plus ONG41008, resulting in the complete inhibition of fibrosis and of autophagosome production (Figure 4A). Western blotting of ONGHEPA1 cell lysates with a cleavage-specific anti-LC3 antibody showed fragmentation of LC3 protein, generating A/B polypeptide fragments (Figure 4B). Taken together, these findings indicate that ONG41008 is a potent anti-inflammatory drug as well as an inductor of autophagy, suggesting that ONG41008 may lessen the severity of IPF or liver inflammation such as NASH.

The therapeutic efficacy of ONG41008 in the treatment of IPF was analyzed in a bleomycin-induced lung fibrosis (BLM) model. Animals were orally administered 10–50mpk ONG41008, with 10 and 25mpk ONG41008, but not 50mpk ONG41008, effectively and significantly blocking the production of soluble collagen (Figure 5A). On the contrary, since 50mpk ONG41008 exhibited the most effective inhibitory capacity on hydroxyproline production. We speculate that the used mice colony for measuring soluble collagen might not properly respond to BLM. Pirfenidone tended to reduce soluble collagen and HP production,

with collagen morphometry showing that 50mpk ONG41008 significantly inhibited the production of collagen and HP (Figure 5B). Furthermore 100mpk pirfenidone and 100mpk ONG41008 consistently inhibited *in vivo* TGFβ production (Supplementary Figure S4A). A therapeutic BLM model was also tested, in which bleomycin was intratracheally administered for 1 week followed by daily oral administration of ONG41008 for 2 weeks. Maximal reduction of collagen production was observed at 50 and 100mpk ONG41008, but no significant inhibition was observed at 10mpk ONG41008 or 100mpk pirfenidone, suggesting that greater exposure to ONG41008 may be needed to cope with existing lung fibrosis. Although 10 and 50mpk ONG41008 tended to reduce the production of HP, 100mpk significantly inhibited HP production (Figure 5C). Expression of αSMA were significantly lower in ONG41008-treated than in control mice. However, dexamethasone did not affect αSMA staining, indicating that anti-inflammatory agents may be unable to mitigate the proliferation of myofibroblasts at advanced stages (Figure 5D).

Lung tissue PK experiments were performed to determine the percentage of parental compounds remaining 1 hr after oral administration 100mpk pirfenidone or ONG41008. The amount of ONG41008 was around ten-fold less than that of pirfenidone, suggesting that disease-correcting signaling associated with a given drug may a be more relevant index of its therapeutic efficacy than residual drug amounts (Supplementary Figure S4B). Taken together, these findings suggest that ONG41008 may be a good candidate for treating IPF, either as monotherapy or in combination with pirfenidone.

The combined anti-inflammatory and anti-fibrotic activities of ONG41008 suggest that this agent may be ideal for the treatment of NASH, a challenging immunometabolic disease characterized by fatty liver, lobular inflammation, hepatocyte ballooning and progressive fibrosis.[4 23] Blockade of inflammation and/or fibrosis may therefore ameliorate NASH. The

STAM mouse model, involving treatment for 5–8 weeks, resembles human NASH.[24] STAM mice were orally administered vehicle, 50mpk ONG41008, 30mpk telmisartan (positive control) or 30mpk obeticholic acid (OCA; negative control). Treatment with 50mpk ONG41008 improved fatty liver, whereas 30mpk OCA had no effect (Figure 6A). ONG41008 at a dose of 50mpk tended to reduce lobular inflammation and hepatocyte ballooning, whereas 30mpk OCA tended to inhibit fibrosis. Telmisartan clearly improved all parameters (Figure 6A and 6B). Pathologic manifestations were given NAFLD scores, with 1 indicating steatosis, two indicating lobular inflammation and three as hepatocyte ballooning and hepatic fibrosis (Figure 6C). Close pathological examination revealed that ONG41008 and telmisartan were therapeutically effective for NASH based on NAFLD scores (Figure 6D).

Considering all these results, we established an integrative view on anti-inflammatory and anti-fibrotic capabilities associated with ONG41008 (Figure 7).

Because we assessed the anti-inflammatory activity of ONG41008 in TGFβ-treated HSCs and DHLFs, it was unclear whether its anti-inflammatory activity was applicable to LPS-treated macrophages in the absence of TGFβ. RAW264.7 cells, a mouse monocytic leukemic cell line resembling macrophages, were stimulated with LPS in the presence or absence of ONG41008. The expression of mRNAs encoding proinflammatory cytokines and chemokines, including *TNFα*, *IL-1β*, *CCL2*, *CCL7*, and *CXCL2*, was markedly downregulated (Figure 8A–E), as was the expression of *CHOP* and *NOX1*, suggesting that ONG41008 inhibits inflammasome formation (Figure 8F,G).[25-27] However, the expression of *IL6* and *IL23* was not significantly reduced (data not shown). TNFα ELISA showed that TNFα protein levels were clearly reduced (Figure 8H). ONG41008 effectively blocked the expression of *TNFα* induced by varying concentrations of LPS, ranging from 100 ng/ml to 10 μg/ml, suggesting that some membrane proximal events may be responsible for the ONG41008-mediated inhibition of

TNFα gene expression (Supplementary Figure S5) and that ONG41008 may inhibit the formation of TLR4-LPS binding proteomes or signalosomes, such as CD14, MD-2 or Myd88.[28] A number of the human TLR family members utilize CD14 as a coreceptor. Assessment of the intracellular trafficking of these proteins upon LPS stimulation showed endocytosis of CD14 alone in response to LPS followed by its redistribution in the plasma membrane (Figure 9A). Magnified views further revealed that endocytosis was coupled with CD14 relocation to the plasma membrane (Supplementary Figures S5A–C). By contrast, MD-2, TLR4, Myd88, and NOX4 remained unaltered (Supplementary Figure S8). In sum, stimulation of RAW264.7 cells with LPS in the presence of ONG41008 resulted in the rapid endocytosis and redistribution of CD14 to the plasma membrane. While LPS rapidly upregulated CD14 treatment with ONG41008 remained unchanging (Figure 9B). Taken together, these findings indicate that ONG41008 is an endocytosis inhibitor of CD14, as illustrated in Figure 9C.

In conclusion, we describe a CS-containing small molecule, ONG41008, with both anti-fibrotic and anti-inflammatory activities. ONG41008 may ameliorate a broad range of fibrotic conditions, such as fibrosis of the heart and kidneys, macular fibrosis, and NASH, as well as fibrotic cancers such as pancreatic cancer. In addition to these generalized anti-inflammation via innate immunity ONG41008 may be an effective modality for autoreactive peripheral or central T cells-mediated hyper inflammation.

Acknowledgments

The authors thank Prof. Ho-Sup Yoon (Nanyang Technological University, Singapore) for insightful comments on the paper. This study was supported by an intramural fund from OsteoNeuroGen.

Competing financial interests

H-S Kim, I-K Kim, and B-S Youn are owners of shares of OsteoNeuroGen, and M-K Meang and MinJu Ham are employed by OsteoNeuroGen. The ONG41008 data are the subject of a Korean patent, an international PCT and a US patent.

Author contributions

B-S Youn and H-S Kim conceived the idea. I-H Kim and B L. Seong coordinated the experiments and helped to write the manuscript. M-K Meang and Mj Ham were largely involved in performing major experiments,

Animal care: The care of mice, rats and beagle dogs care was managed by the IACUC associated with Syngene International (Bangalore, India).

Footnotes:

The following abbreviations are used throughout this manuscript;

CS: Chromone scaffold

CD: Chromone scaffold derivatives

IPF: Idiopathy pulmonary fibrosis

BILF: Bleomycin-induced lung fibrosis

NASH: Nonalcoholic steatohepatitis

DHLFs: Diseased human lung fibroblasts

References

1. Meyer, K.C. Pulmonary fibrosis, part I: epidemiology, pathogenesis, and diagnosis. *Expert Rev. Respir. Med.* **11**, 343-359 (2017).
2. Raghu, G., *et al.* Idiopathic Pulmonary Fibrosis: Prospective, Case-Controlled Study of Natural History and Circulating Biomarkers. *Chest* **154**, 1359-1370 (2018).
3. Wattacheril, J., Issa, D. & Sanyal, A. Nonalcoholic steatohepatitis (NASH) and hepatic fibrosis: Emerging therapies. *Ann. Rev. Pharmacol. Toxicol.* **58**, 649-662 (2018).
4. Bessone, F., Razori, M.V. & Roma, M.G. Molecular pathways of nonalcoholic fatty liver disease development and progression. *Cell. Mol. Life Sci.* **76**, 99-128 (2019).
5. Marra, F. & Lotersztajn, S. Pathophysiology of NASH: perspectives for a targeted treatment. *Curr. Pharm. Des.* **19**, 5250--5269 (2013).
6. Maher, T.M., *et al.* Unmet needs in the treatment of idiopathic pulmonary fibrosis-insights from patient chart review in five European countries. *BMC Pulm. Med.* **17**, 124 (2017).
7. Kim, H.S., *et al.* Reversion of in vivo fibrogenesis by novel chromone scaffolds. *EBioMedicine* **39**, 484-496 (2019).
8. King, C.S. & Nathan, S.D. Practical considerations in the pharmacologic treatment of idiopathic pulmonary fibrosis. *Curr. Opin. Pulm. Med.* **21**, 479-489 (2015).
9. Dixon, R.A. & Pasinetti, G.M. Flavonoids and isoflavonoids: From plant biology to agriculture and neuroscience. *Plant Physiol.* **154**, 453-457 (2010).
10. Stapleton, A.E. & Walbot, V. Flavonoids can protect maize DNA from the induction of ultraviolet radiation damage. *Plant Physiol.* **105**, 881-889 (1994).
11. Leyva-López, N., Gutierrez-Grijalva, E.P., Ambriz-Perez, D.L. & Heredia, J.B. Flavonoids as cytokine modulators: A possible therapy for inflammation-related diseases. *Int. J. Mol. Sci.* **17**, 921 (2016).

12. Emami, S. & Ghanbarimasir, Z. Recent advances of chroman-4-one derivatives: synthetic approaches and bioactivities. *Eur. J. Med. Chem.* **93**, 539-563 (2015).

13. Gacche, R.N., *et al.* Flavonoids as a scaffold for development of novel anti-angiogenic agents: An experimental and computational enquiry. *Arch. Biochem. Biophys.* **577-578**, 35=48 (2015).

14. Kim, J.Y., *et al.* Massive elimination of multinucleated osteoclasts by eupatilin is due to dual inhibition of transcription and cytoskeletal rearrangement. *Bone Rep.* **3**, 83-94 (2015).

15. Makarev, E., *et al.* Common pathway signature in lung and liver fibrosis. *Cell Cycle* **15**, 1667-1673 (2016).

16. Wang, Y., *et al.* Unsupervised gene expression analysis identify IPF-severity correlated signatures, associated genes and biomarkers. *BMC Pulm. Med.* **17**, 133 (2017).

17. Mullenbrock, S., *et al.* Systems analysis of transcriptomic and proteomic profiles identifies novel regulation of fibrotic programs by miRNAs in pulmonary fibrosis fibroblasts. *Genes (Basel)* **9**, pii: E588 (2018).

18. Singh, A., *et al.* NADPH oxidase 4 modulates hepatic responses to lipopolysaccharide mediated by Toll-like receptor-4. *Sci. Rep.* **7**, 14346 (2017).

19. Weiskirchen, R. & Tacke, F. Cellular and molecular functions of hepatic stellate cells in inflammatory responses and liver immunology. *Hepatobiliary Surg. Nutr.* **3**, 344-363 (2014).

20. Higashi, T., Friedman, S.L. & Hoshida, Y. Hepatic stellate cells as key target in liver fibrosis. *Adv. Drug Deliv. Rev.* **121**, 27-42 (2017).

21. Liu, T., *et al.* Alleviation of hepatic fibrosis and autophagy via inhibition of transforming growth factor-β1/Smads pathway through shikonin. *J. Gastroenterol. Hepatol.* **34**, 263-276 (2019).

22. Hill, C., *et al.* Autophagy inhibition-mediated epithelial-mesenchymal transition augments local myofibroblast differentiation in pulmonary fibrosis. *Cell Death Dis.* **10**, 591 (2019).

23. Monteiro, P.A., *et al.* Immunometabolic Changes in Hepatocytes Arising from Obesity and the Practice of Physical Exercise. *Curr. Pharm. Des.* **24**, 3200-3209 (2018).

24. Saito, K., *et al.* Characterization of hepatic lipid profiles in a mouse model with nonalcoholic steatohepatitis and subsequent fibrosis. *Sci. Rep* **5**, 12466 (2015).

25. Grant, R., *et al.* Inactivation of C/ebp homologous protein-driven immune-metabolic interactions exacerbate obesity and adipose tissue leukocytosis. *J. Biol. Chem.* **289**, 14045-14055 (2014).

26. Sun, B., *et al.* NADPH Oxidase-Dependent NLRP3 Inflammasome activation and its important role in lung fibrosis by multiwalled carbon nanotubes. *Small* **11**, 2087-2097 (2015).

27. Zhang, L.L., *et al.* Angiotensin(1-7) attenuated Angiotensin II-induced hepatocyte EMT by inhibiting NOX-derived H2O2-activated NLRP3 inflammasome/IL-1β/Smad circuit. *Free Radic. Biol. Med.* **97**, 531-543 (2016).

28. Cheng, Z., Taylor, B., Ourthiague, D.R. & Hoffmann, A. Distinct single-cell signaling characteristics are conferred by the MyD88 and TRIF pathways during TLR4 activation. *Science Signaling* **8**, ra69 (2015).

Figure legends

Fig. 1. ONG41008 inhibits fibrosis in both lung fibroblasts and hepatic stellate cells. (A) ONGHEPA1 and (B) DHLF cells were incubated for 24 hr with medium (GM), TGFβ, or TGFβ, with or without ONG41008, followed by immunocytochemical staining for α-SMA and viewing under a fluorescent microscope. *Periostin, collagen1α1, collagen11α1*, and *AURKA* mRNA levels were measured in parallel by qPCR in parallel. (C) Kinetics of ONG41008 induction of SMAD and ERK phosphorylation in the presence of TGFβ. ONGHEPA1 cells were treated with TGFβ, with or without ONG41008, for 0, 5, 15, 30, 45, 60, and 120 mins, and protein expression was analyzed by western blotting. (D) Actin-phalloidin staining to test actin depolymerization. DHLFs were treated with TGFβ and ONG41008, pirfenidone, or nintedanib and observed under the microscope. (E) In vitro actin polymerization and (F) depolymerization assay. Cells were incubated with various concentrations of ONG41008, and actin polymerization activity and amount of depolymerization were measured by kinetic mode fluorometry. *$P < 0.05$, **$P<0.01$, by Student's t-tests. (G,H) Latent complex proteins in (G) DHLF and (H) ONGHEPA1 cells, as assessed by ICC, with ONGHEPA1 cells also stained with phalloidin.

Fig. 2. Transcriptomics analysis showing 77 TGFβ-induced FIGS, including NOX4, significantly downregulated by ONG41008. (A) Schematic representation of transcriptome selection in cells treated with TGFβ and TGFβ plus ONG41008. (B) List of 77 ONG41008 suppressible FIGS. (C) Interactome study using STRING database of the 77 listed FIGS. Of these 77 genes, 28 appeared to be isolated from the major interactome. Twenty-eight unconnected genes were deleted to better visualize connectivity.

Fig. 3. NOX4, CCL2 and CCL7 are induced by TGFβ and blocked by ONG41008. (A) qPCR of *Collagen11α1*, *Periostin* and *NOX4* mRNAs expressed by ONGHEPA1 cells treated with TGFβ for 0, 6, 9, 12, and 24 hr. (B, C) ICC for NOX4 protein expressed by (B) ONGHEPA1 and (C) DHLF cells incubated for 24 hr with GM, TGFβ, or TGFβ plus ONG41008. (D) ROS assay using DCFDA of ONGHEPA1 cells incubated as in (B). (E) qPCR of *NOX4*, *CCL2*, and *CCL7* mRNAs expressed by ONGHEPA1 cells incubated as in (B).

Fig. 4. ONG41008 induces autophagosome formation in DHLF and ONGHEPA1 cells. (A) ICC staining of ONGHEPA1 and DHLF cells, showing small puncta in cells treated with TGFβ plus ONG41008 but in cells treated with TGFβ alone. (B) ONGHEPA1 cells were treated with TGFβ or TGFβ plus ONG41008 for 0, 5, 15, 30, 45, 60, and 120 mins, followed by western blotting using antibodies against the autophagy markers LC3 A/B and P62.

Fig. 5. ONG41008 had positive effects against lung fibrosis in both BLM prevention and therapeutic models. (A, C) Lung collagen and hydroxyproline levels measured after treatment with pirfenidone or 10, 25, or 50 mg/kg ONG41008 in the (A) BLM prevention and (C) BLM therapeutic models. Percent inhibition relative to vehicle control is shown in blue characters, with average measurements in black. (B) Masson's Trichome staining of lung sections in the BLM prevention model. (D) Staining of lung sections with anti-αSMA staining antibody in the BLM therapeutic model. ***P < 0.001, relative to Sham, and $P < 0.05, $$$P < 0.001 relative to vehicle control by Student's t-tests.

Fig. 6. ONG41008 had positive effects against NASH and NAFLD in the STAM mouse model. (A, B) H&E staining of liver sections of hepatectomized STAM mice treated with telmisartan, OCA or ONG41008. (C) Scoring for signs of hepatic steatosis, lobular

inflammation and hepatocyte ballooning under each condition. (D) NAFLD activity score charted for ONG41008 and controls. Statistical significance was calculated by Student's t-test.

Fig. 7. Mode of action of ONG41008. ONG41008 disrupts actin stress filaments by depolymerization of F-actin, dismantling latent TGFβ complexes. The inability of TGFβ to bind to TGFβ I and II signaling receptors prevents the generation of canonical or noncanonical TGFR signaling, leading to the attenuation of type 2 EMT. ONG41008 also blocks the phosphorylation of SMAD 2/3. These two mechanisms may be responsible for efficiently preventing myofibroblast production of collagen and/or hydroxyproline. Its inhibition of NOX4 and induction of autophagy suggest that ONG41008 may also prevent fibrosis and promote cellular homeostasis, such as cell survival, as well as having anti-steatosis properties and lowering insulin resistance.

Fig. 8. Inhibition of LPS activated genes by ONG41008 in RAW264.7 cells. (A-G) RAW264.7 cells were stimulated with LPS (100 ng/ml) or LPS plus ONG41008 (25 μM or 50 μM) for 24 hr and mRNA expression of inflammatory markers was measured by qPCR. (H) Cell supernatants at each condition were collected and the concentrations of secreted TNFα (pg/ml) were measured by ELISA. Each resent is representative of three independent experiments. *$P < 0.05$, **$P < 0.01$, ***$P < 0.001$ by Student's t-tests.

Fig. 9. ONG41008 is an endocytosis inhibitor of CD14. (A) ICC for CD14 in RAW264.7 cell incubated with GM, LPS or LPS plus ONG41008. (B) Western blot of CD14 in RAW264.7 cells incubated with LPS or LPS plus ONG41008 for 0, 5, 15, 30, 45, 60, and 120 mins. (C) Anti-inflammatory mode of action of ONG41008. LPS-LBP binds to the COOH-terminal region of CD14. Formation of these trimeric complexes may directly prevent the endocytosis

of CD14, whereas the MD-2-TLR4 complex was not redistributed in LPS-stimulated RAW264.7 cells.

Materials and Methods

Cell culture and reagents

DHLFs were purchased from Lonza (Basel, Switzerland) and cultured in fibroblast growth medium (FBM, Lonza, Walkersville, MD, USA). Recombinant human TGF-β and PDGF were obtained from Peprotech (Rocky Hill, CT, USA) and used at final concentrations of 5 ng/ml. Chemically synthesized ONG41008 was obtained from Syngene International Ltd. (Bangalore, India), dissolved at a stock concentration of 50 mM in DMSO, and stored in aliquots at -20°C. DMSO with was used as control. RAW264.7 cells were purchased from the Korean Cell Line Bank (Seoul, Korea) and cultured in RPMI supplemented with 10% FBS and 1% P/S (Welgene, Seoul, Korea). LPS was purchased from Sigma and used at a final concentration of 100 ng/ml.

Effects of drugs on bleomycin-induced lung tissue fibrosis

C57BL/6J mice were anesthetized by inhalation of 70% N_2O and 30% O_2 gas containing 1.5% isoflurane. Fifty microliters of bleomycin solution in distilled water was directly injected into their lungs via the aperture. The mice were allowed to recover from the anesthetic and then housed in normal cages. Bleomycin (0.03 U in 50 µl saline) was administered once using a visual instillobot. Seven days after the administration of bleomycin, mice were orally administered with 10 to 100mpk ONG41008 dissolved in 0.5% CMC containing 1% Tween80 via a micropipette, once daily for 2 weeks. For 2 to 3 days after administration of eupatilin, the mice were monitored for toxic symptoms or death, but no abnormal symptoms were observed. One hour before sacrifice, a final dose of ONG41008 or pirfenidone was administered for plasma or lung PK. Ten mice per test group were selected, and their lung tissues were excised, stained with Masson's trichrome and observed under a microscope. Results were expressed as mean and standard deviation. Data from control and eupatilin-

treated mice were compared using Student's *t*-test, with $p<0.05$ considered statistically significant.

RNA-seq processing, differential gene expression analysis, and interactome analysis

Processed reads were mapped to the *Mus musculus* reference genome (Ensembl 77) using Tophat and Cufflink with default parameters. Differential analysis was performed using Cuffdiff with default parameters. FPKM values from Cuffdiff were normalized and quantitated using the R Package Tag Count Comparison (TCC) to determine statistical significance (P values) and differential expression (fold changes). Gene expression was plotted as fold-changes using Scatter, MA, and Volcano plots, using an R script developed in-house. The protein interaction transfer procedure for the differentially expressed genes was performed using the STRING database. A 60 Gb sequence was generated, and 10,020 transcripts were read and compared. The highest-confidence interaction score (0.9) was applied from *Mus musculus*, and information about interacts were obtained based on text mining, experiments, and databases (http://www.string-db.org/).

Reverse transcriptase PCR and real-time PCR

Cells cultured in either 12- or 24-well plates were washed twice with cold PBS and harvested using TaKaRa MiniBEST Universal RNA extraction kits (Takara, Japan). Total RNA was purified using the same kits according to the manufacturer's protocol. RNA was reverse-transcribed using cDNA Synthesis Kits (PCRBio Systems, London, UK), followed by amplification with StepOne Plus (Applied Biosystems, Life Technologies) and 2× qPCRBio Probe Mix Hi-ROX (PCRBio). mRNA levels were compared using the ΔΔCt method, with GAPDH mRNA as the internal control.

ELISA and immunoblotting

Mouse TNFα Quantine ELISA kits were purchased from R&D Systems (Minneapolis, MN, USA). Raw264.7 cells were seeded at 1×10^5 cells/well in 12-well cell culture plates and incubated overnight, followed by treatment with 100 ng/ml LPS and various concentrations of ONG41008, with a balancing amount of DMSO added to each well. After 24 hr, the supernatants were collected, and ELISA performed as according to the manufacturer's instructions. Standard curves were constructed during each experiment to calculate TNFα concentrations. For western blotting, antibodies to CD14, MD-2, P62, and GAPDH were purchased from Abcam (Cambridge, UK); antibodies to MyD88, TLR4 from R&D Systems, antibody to NOX4 (14347-1-AP) from Proteintech (Rosemont, IL, USA), and antibodies to LC3 A/B, pSMAD-2, pSMAD-3, SMAD2/3, pERK 1/2, and ERK 1/2 from Cell Signaling Technology (Danvers, MA, USA). All antibodies were 1:1000 (v/v) in DPBS containing 5% BSA (Welgene).

Immunocytochemistry

Cells were fixed with 4% paraformaldehyde, permeabilized with 0.3% TritonX100, blocked and incubated with 1:500 dilutions of antibodies to α-SMA (Young In Frontier, Korea), actin-phalloidin (Thermo Fisher, USA), LTBP1 (Aviva Systems Biology, San Diego, USA), LTBP4 (Aviva Systems Biology), LAP1 (Abcam), integrin α5β3 (biorbyt, Cambridge, UK), NOX4 (Proteintech), CD14 (Abcam), MyD88 (R&D Systems), TLR4 (R&D Systems) and MD-2 (Abcam), followed by incubation with a 1:200 FITC-conjugated secondary antibody (Young In Frontier) and imaging with an fluorescence microscope (Thermo). Nuclei were stained with DAPI.

ROS staining

ONGHEAPA1 cells were incubated with TGFβ (5 ng/ml) or TGFβ plus ONG41008 (50 μM), followed by incubation with 10 μM H2DCFDA (Abcam) for 1 hr in the dark at 37°C. Intracellular production of ROS was detected by examining the cells by fluorescence microscopy.

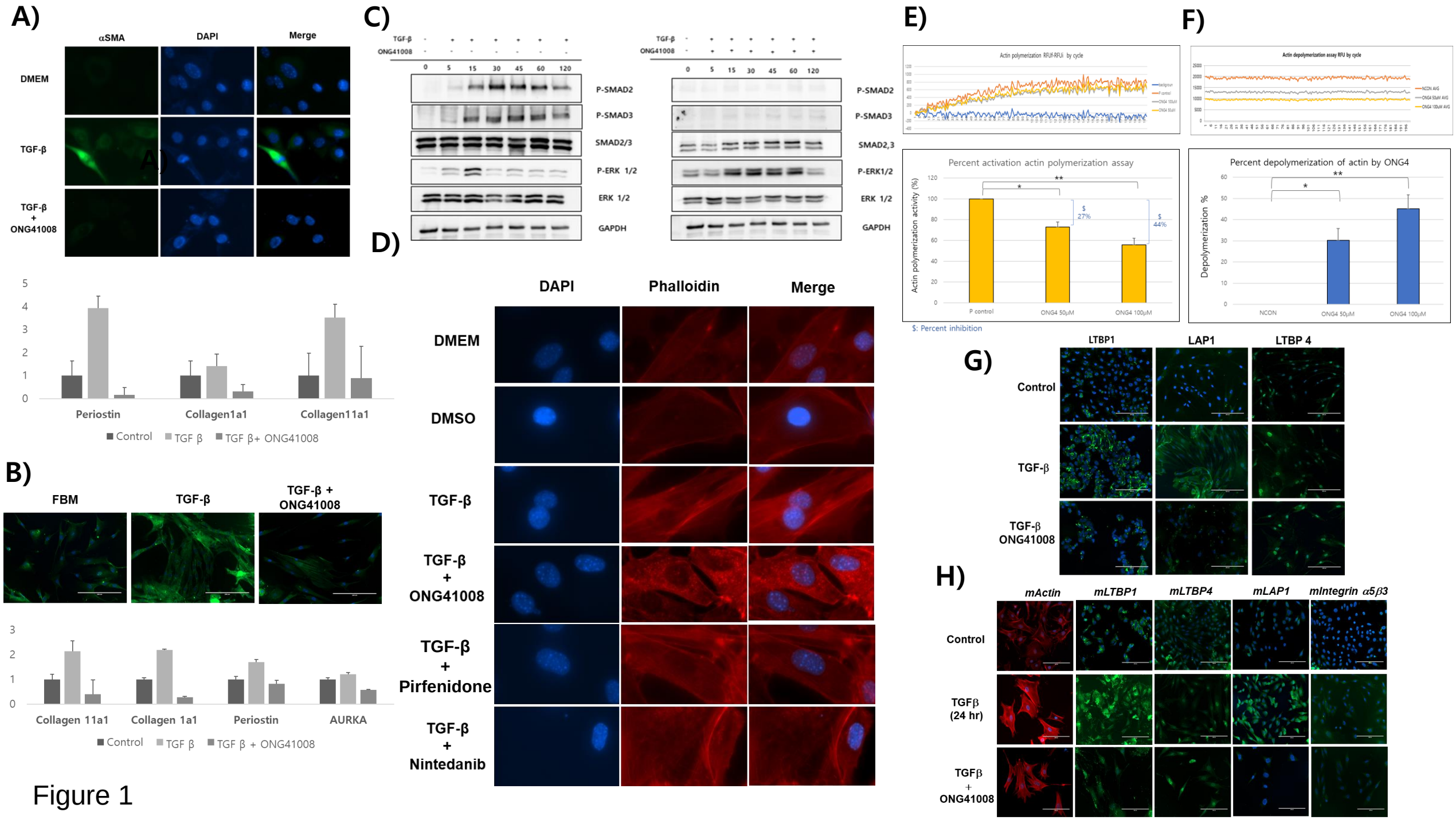
A)
αSMA
DAPI
Merge
DMEM
TGF-β
TGF-β + ONG41008
5
4
3
2
1
0
Periostin
Collagen1a1
Collagen11a1
Control
TGF β
TGF β+ ONG41008
B)
FBM
TGF-β
TGF-β + ONG41008
3
2
1
0
Collagen 11a1
Collagen 1a1
Periostin
AURKA
Control
TGF β
TGF β + ONG41008
C)
TGF-β
ONG41008
0
5
15
30
45
60
120
P-SMAD2
P-SMAD3
SMAD2/3
P-ERK 1/2
ERK 1/2
GAPDH
SMAD2,3
P-ERK1/2
D)
DAPI
Phalloidin
Merge
DMEM
DMSO
TGF-β
TGF-β + ONG41008
TGF-β + Pirfenidone
TGF-β + Nintedanib
E)
Actin polymerization RFUf-RFUi by cycle
Percent activation actin polymerization assay
Actin polymerization activity (%)
120
100
80
60
40
20
0
P control
ONG4 50μM
ONG4 100μM
$: Percent inhibition
F)
Actin depolymerization assay RFU by cycle
Percent depolymerization of actin by ONG4
Depolymerization %
60
50
40
30
20
10
0
NCON
ONG4 50μM
ONG4 100μM
G)
LTBP1
LAP1
LTBP 4
Control
TGF-β
TGF-β ONG41008
H)
mActin
mLTBP1
mLTBP4
mLAP1
mIntegrin α5β3
Control
TGFβ (24 hr)
TGFβ + ONG41008

Figure 1

A)

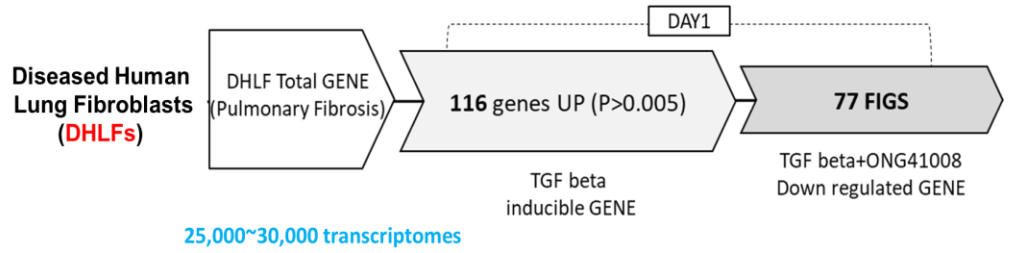

B)

Fibrosis-Inducing Genes (FIGS)

Human DHLFs regulated by ONG41008 via RNA-Seq / p< 0.005

EPHB2	PAWR
LEPRE1	APCDD1L
KIF26B	GALNT10
PLXDC2	PKP1
ANKRD1	PXDC1
POSTN	GJA1
XYLT1	NTM
FAM101B	SH3PXD2A
CDH2	LEPREL4
PXDN	PODXL
COL7A1	PSAT1
PCDH10	NOX4
CDH6	RP11-180C1.1
SPOCK1	FBLN5
EDN1	ADAM19
CTGF	MRC2
IGFBP3	COL1A1
LRRC17	WWTR1
PLAT	LOX
CTHRC1	ITGB5
COL5A1	HHAT
NEGR1	KSR1
VDR	HMCN1
COL4A1	GATA6
TPM1	CDK6
COL11A1	P4HA2
FAM46A	EFEMP1
EDIL3	ALDH1L2
ELN	SLC38A5
DKK1	SEMA7A
TCF4	FIBCD1
PLOD2	NCOA3
NEK7	P4HA1
	ATP10A
	PYCR1
	RNF152
	HAPLN1
	COL5A2
	DGKI
	HYOU1
	ASXL3
	SERPINH1
	SOX2-OT

"NOX4"

77 FIGS

C)

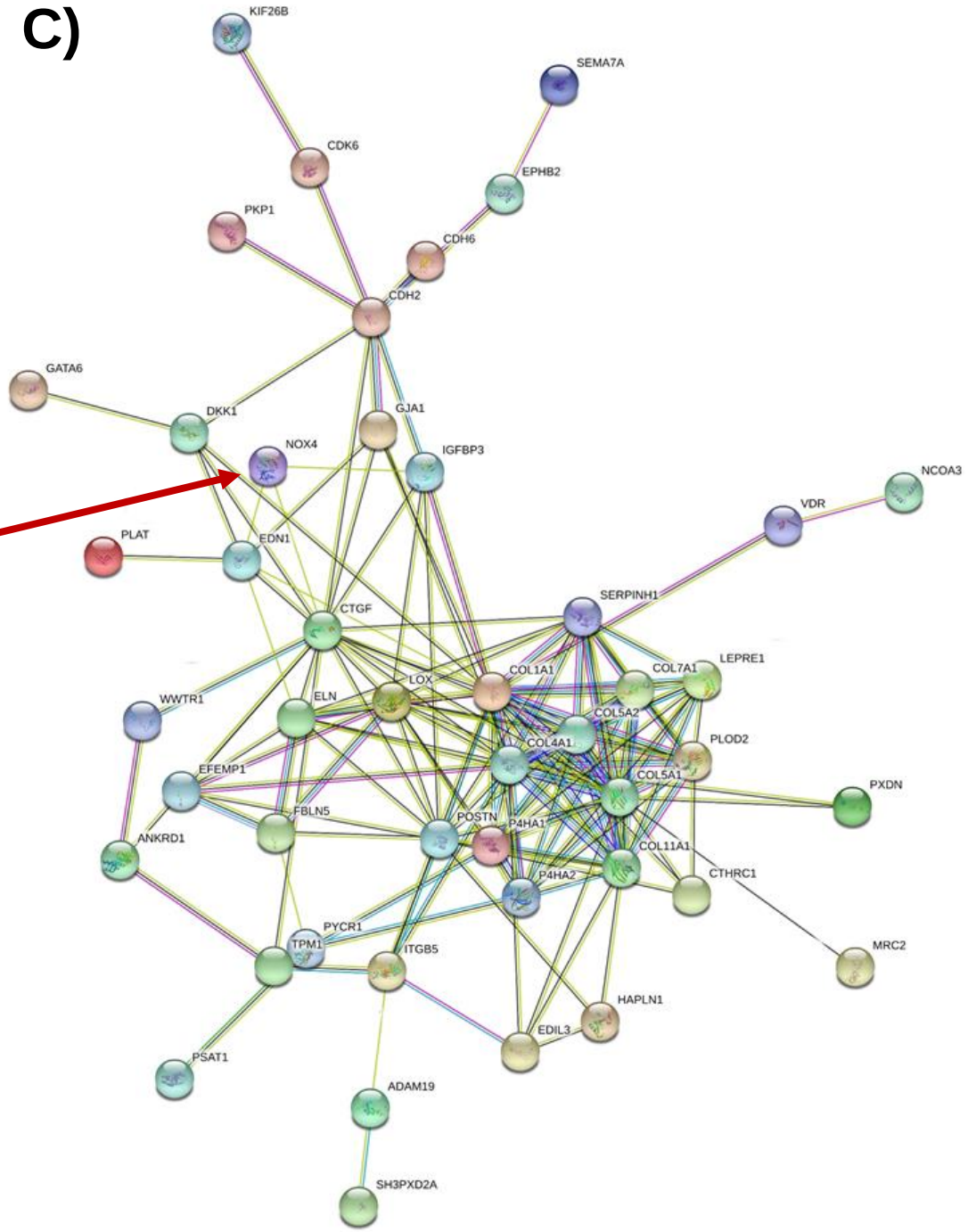

Figure 2

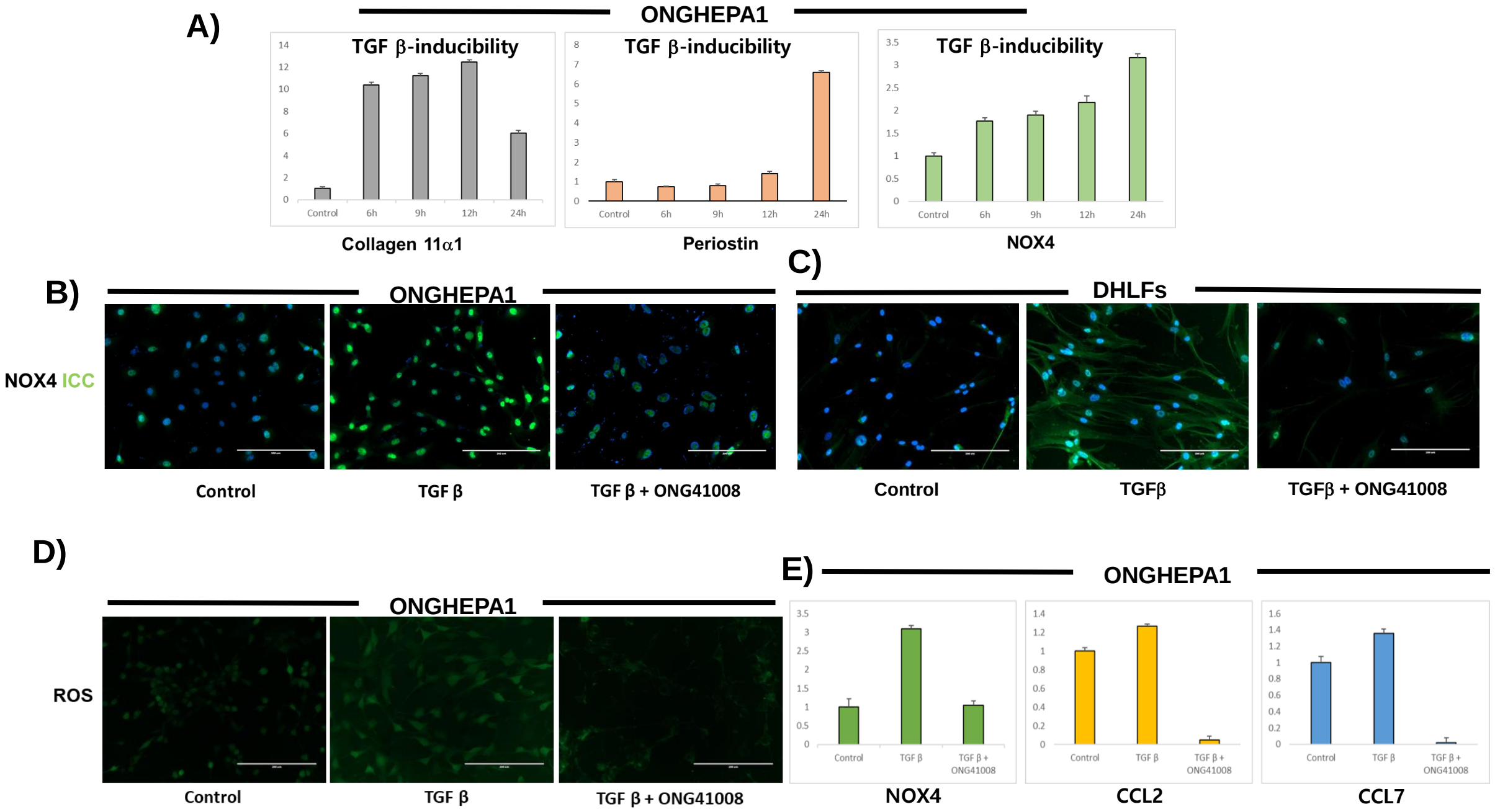
A)
ONGHEPA1
TGF β-inducibility
Control
6h
9h
12h
24h
Collagen 11α1
Periostin
NOX4
B)
ONGHEPA1
NOX4 ICC
Control
TGF β
TGF β + ONG41008
C)
DHLFs
Control
TGFβ
TGFβ + ONG41008
D)
ONGHEPA1
ROS
Control
TGF β
TGF β + ONG41008
E)
ONGHEPA1
NOX4
CCL2
CCL7

Figure 3

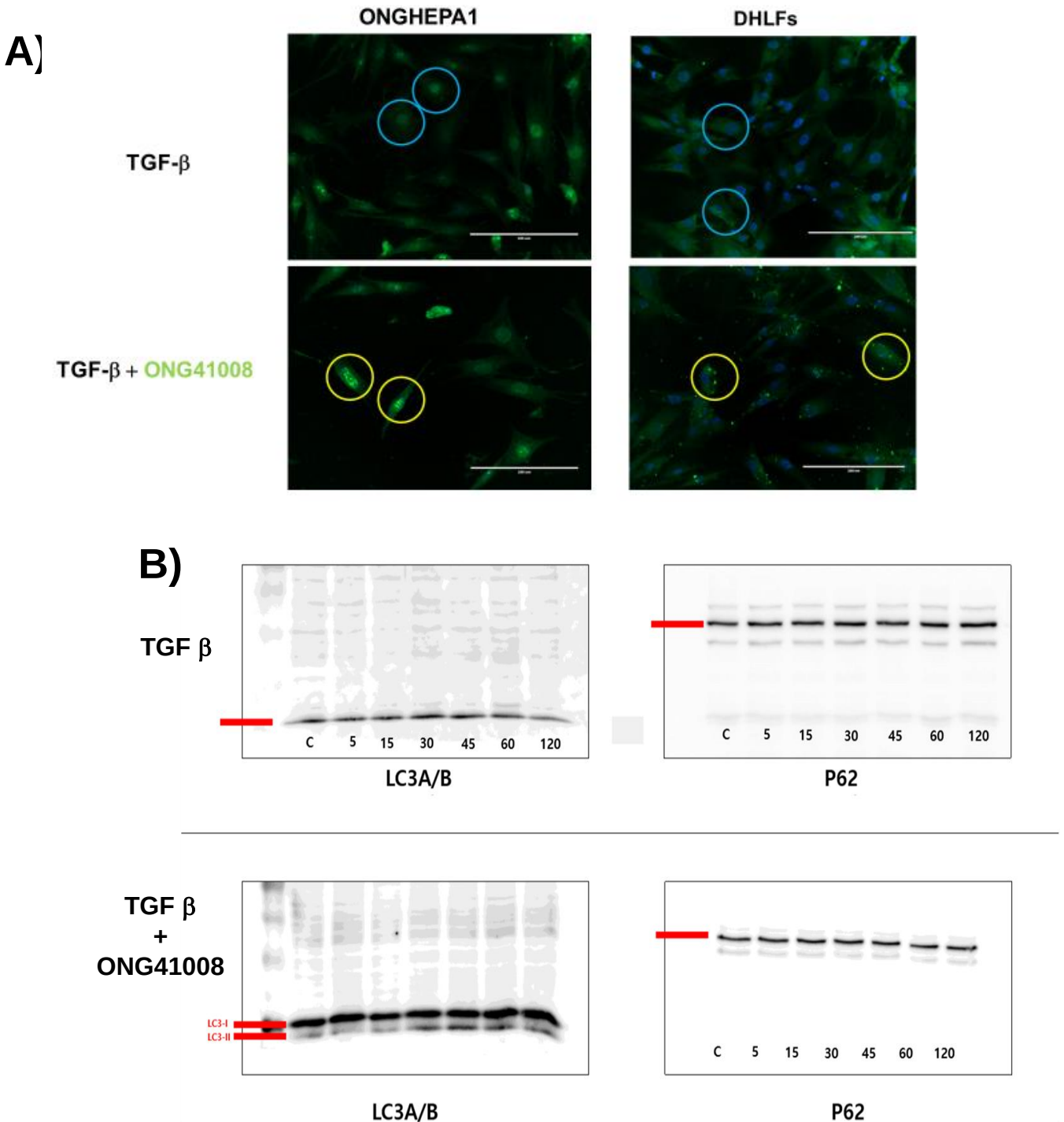
A)
ONGHEPA1
DHLFs
TGF-β
TGF-β + ONG41008
B)
TGF β
C 5 15 30 45 60 120
LC3A/B
C 5 15 30 45 60 120
P62
TGF β
+
ONG41008
LC3-I
LC3-II
LC3A/B
C 5 15 30 45 60 120
P62

Figure 4

A) BLM prevention model

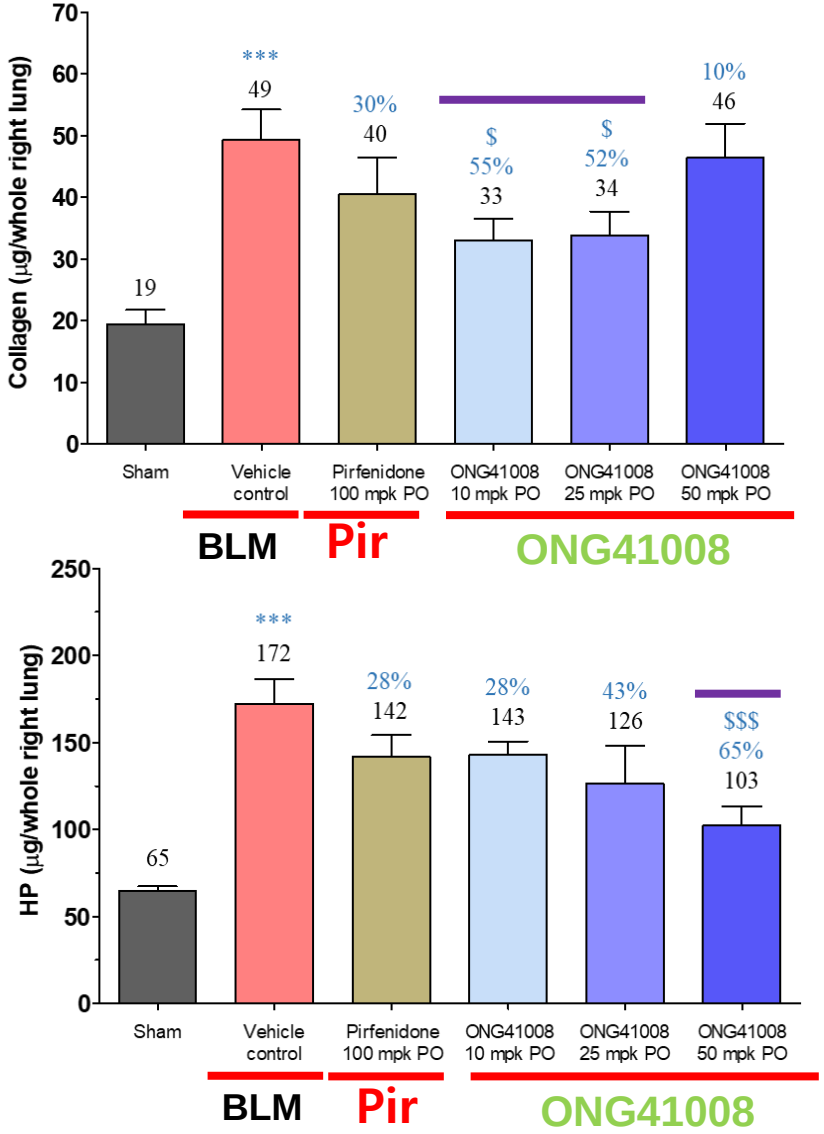

B) Masson's Trichome-stained lung sections

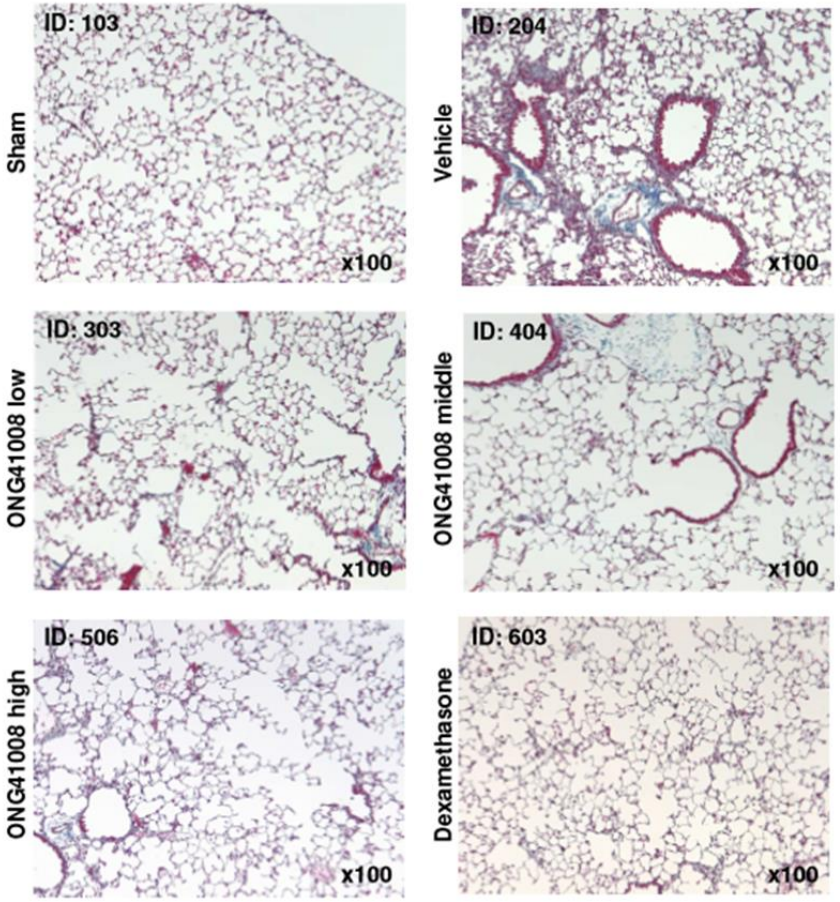

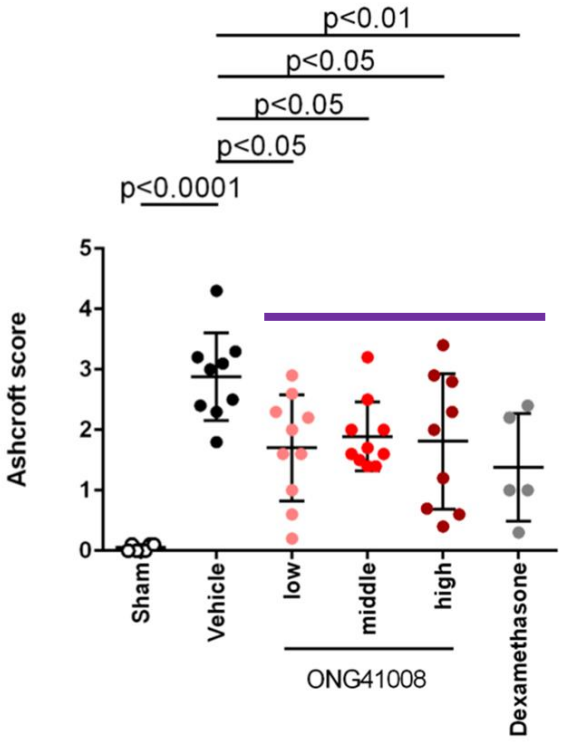

Low: ONG41008 10mpk
Middle: ONG41008 25mpk
High: ONG41008 50mpk
Dexamethasone 0.25mpk

Figure 5

C) BLM therapeutic model

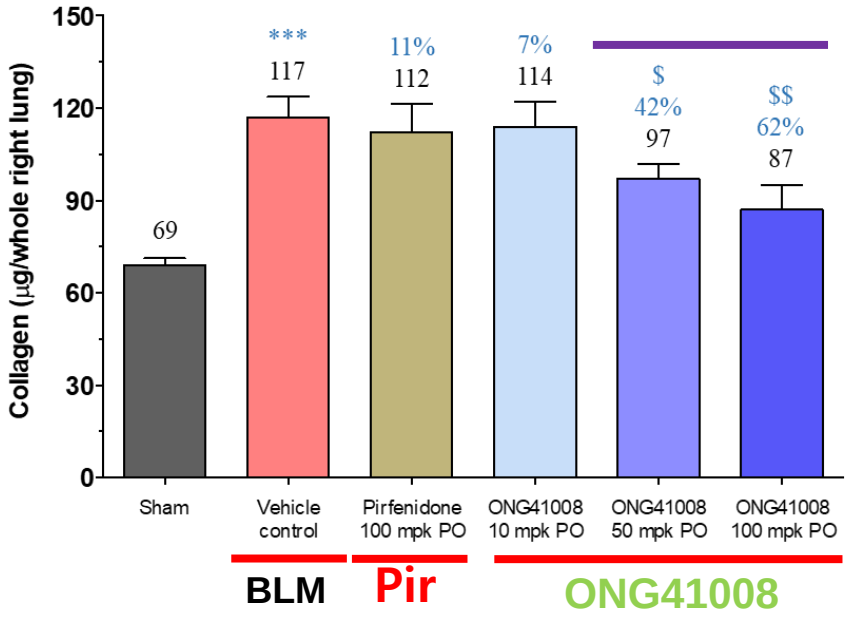

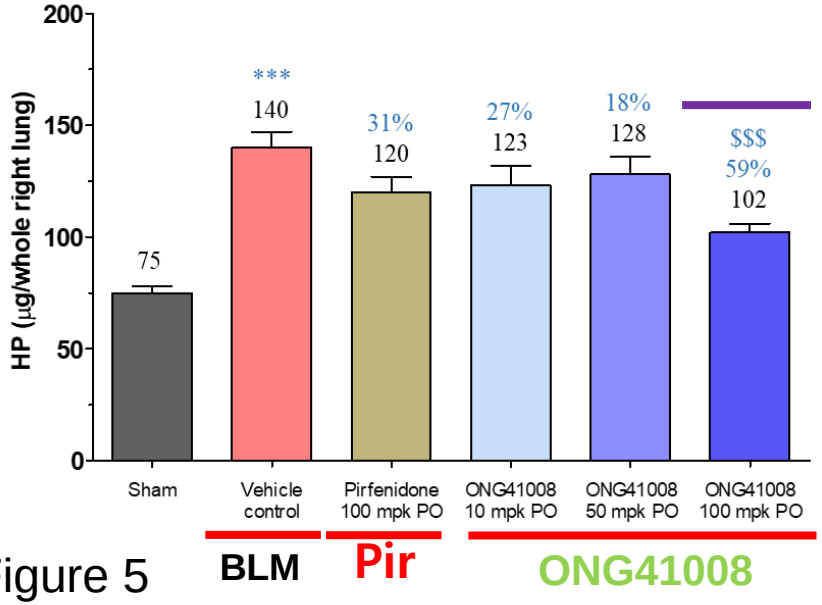

D) *αSMA* staining

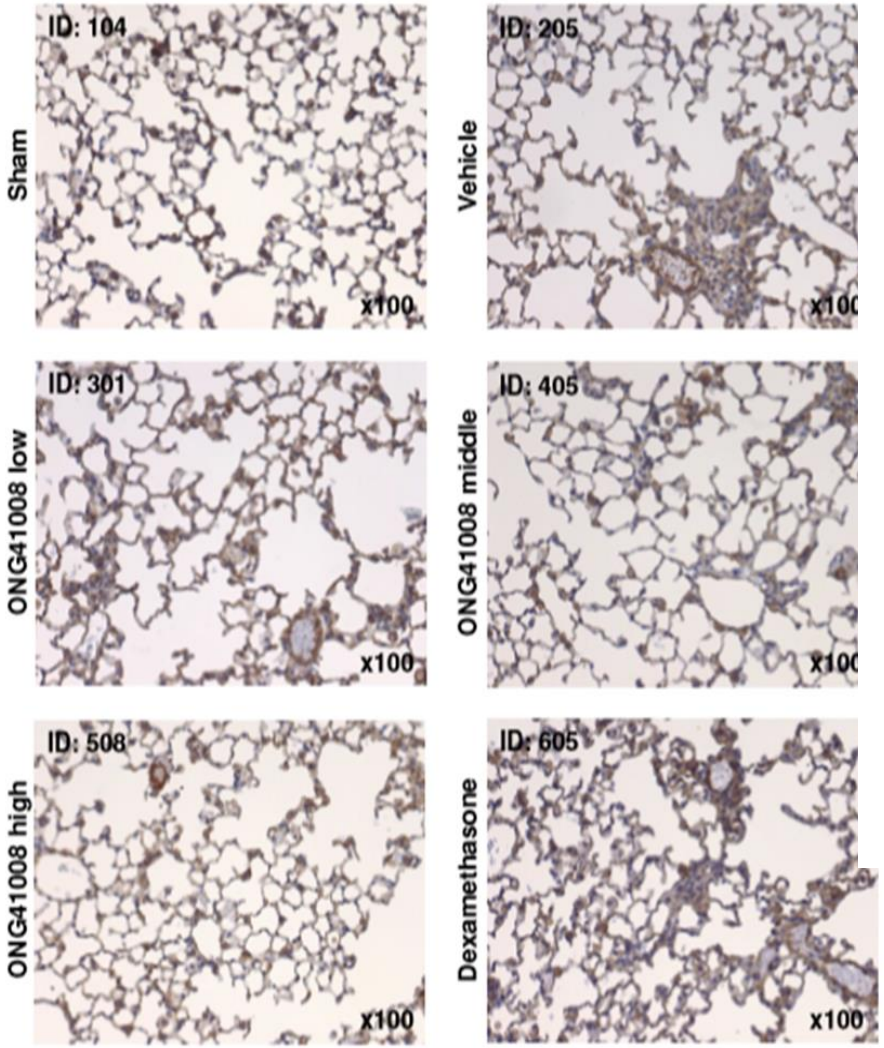

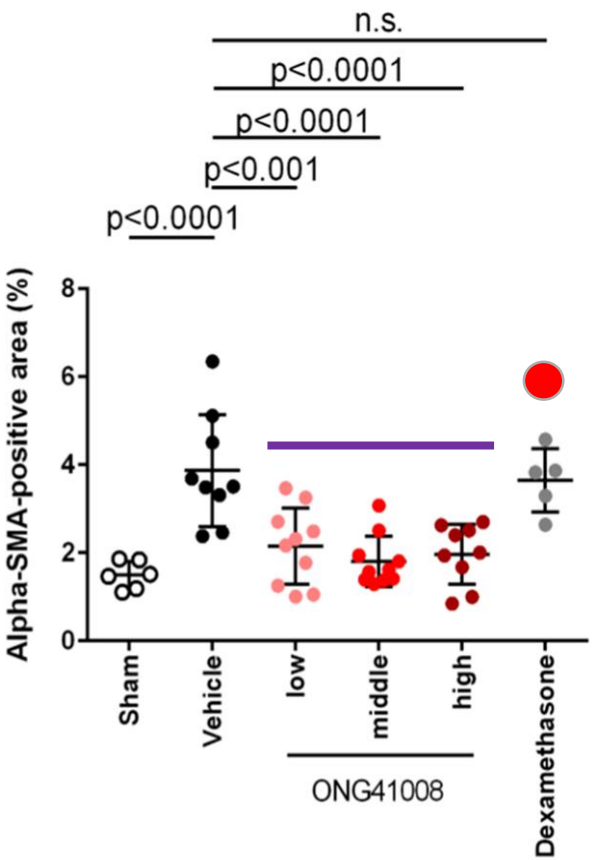

Low: ONG41008 10mpk
Middle: ONG41008 25mpk
High: ONG41008 50mpk
Dexamethasone 0.25mpk

Figure 5

A)

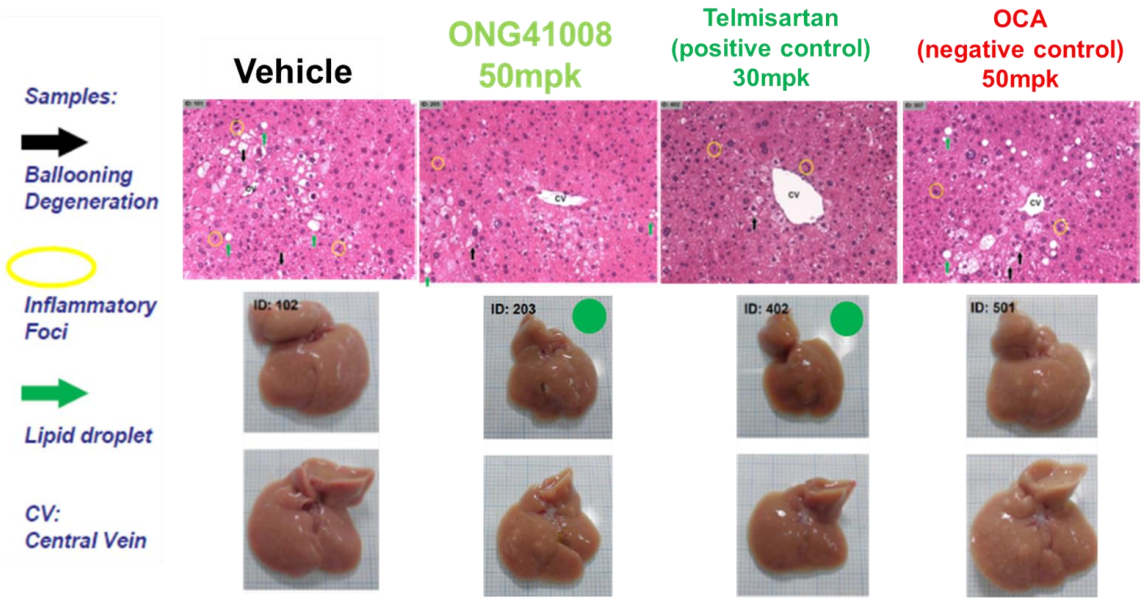

B)

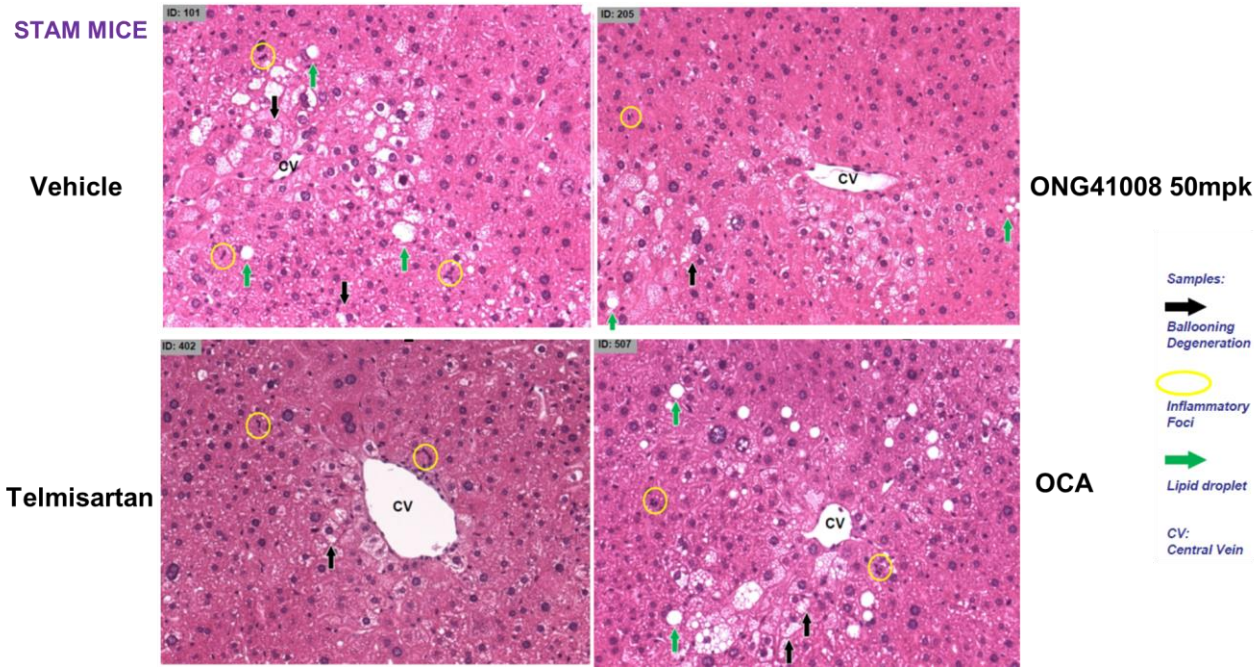

C)

Group	n	Score											NAS (mean ± SD)
		Steatosis				Lobular inflammation				Hepatocyte ballooning			
		0	1	2	3	0	1	2	3	0	1	2	
Vehicle	8	3	5	-	-	-	-	2	6	1	5	2	4.5 ± 0.8
ONG41008	6	3	3	-	-	-	1	2	3	3	2	1	3.5 ± 0.8
Telmisartan	7	5	2	-	-	-	1	5	1	2	4	1	3.1 ± 1.2
OCA	8	3	5	-	-	-	-	6	2	2	4	2	3.9 ± 1.1

Definition of NAS Components

Item	Score	Extent
Steatosis	0	<5%
	1	5-33%
	2	>33-66%
	3	>66%
Lobular Inflammation	0	No foci
	1	<2 foci/200x
	2	2-4 foci/200x
	3	>4 foci/200x
Hepatocyte Ballooning	0	None
	1	Few balloon cells
	2	Many cells/prominent ballooning

D)

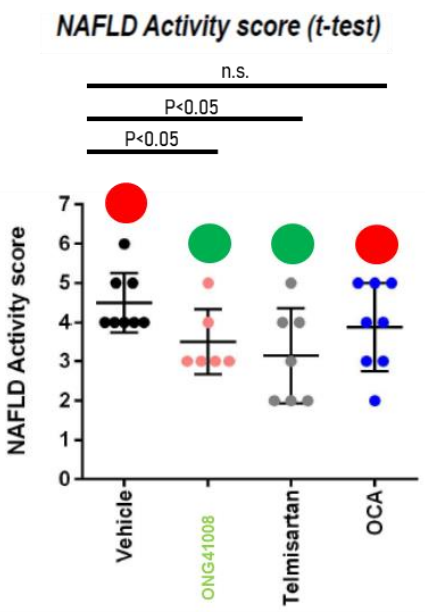

Figure 6

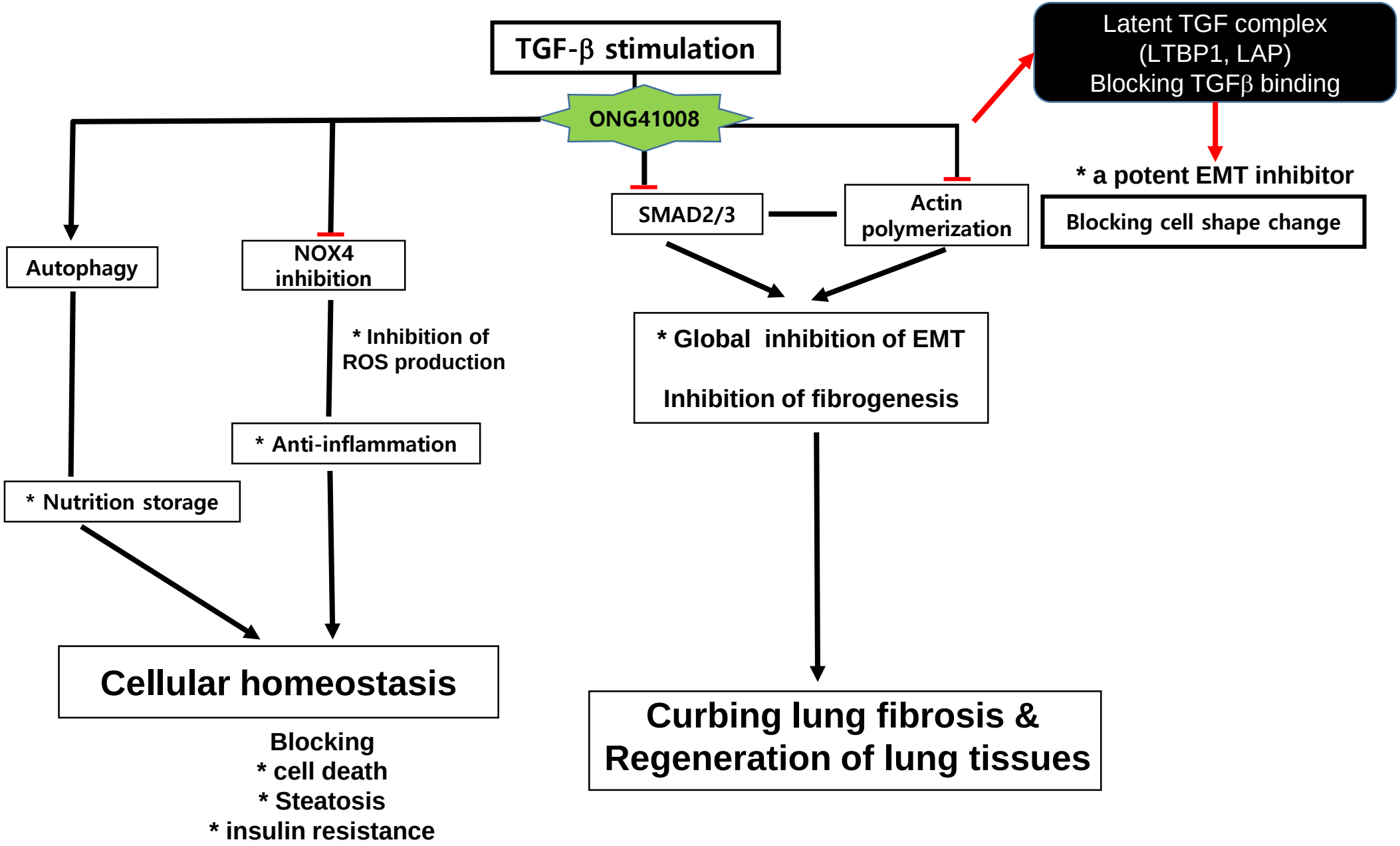
TGF-β stimulation
ONG41008
Latent TGF complex
(LTBP1, LAP)
Blocking TGFβ binding
* a potent EMT inhibitor
Blocking cell shape change
SMAD2/3
Actin polymerization
Autophagy
NOX4 inhibition
* Inhibition of ROS production
* Anti-inflammation
* Nutrition storage
* Global inhibition of EMT
Inhibition of fibrogenesis
Cellular homeostasis
Blocking
* cell death
* Steatosis
* insulin resistance
Curbing lung fibrosis &
Regeneration of lung tissues

Figure 7

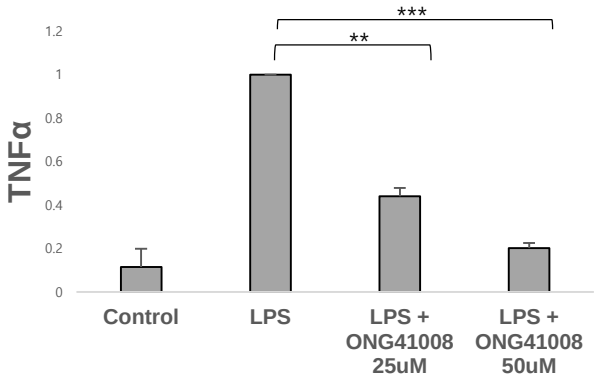

(A)

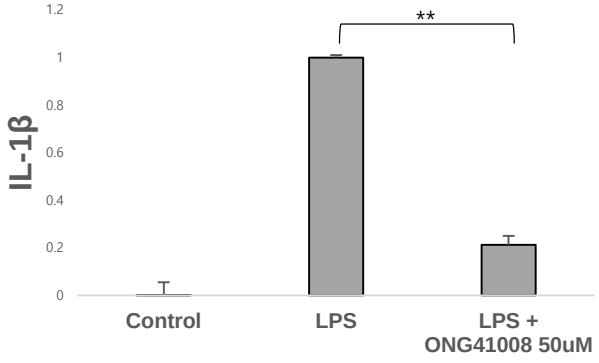

(B)

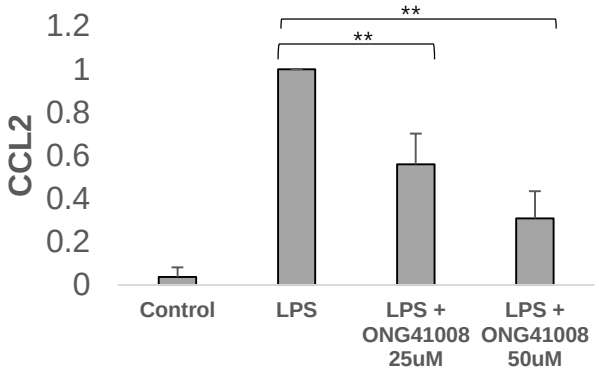

(C)

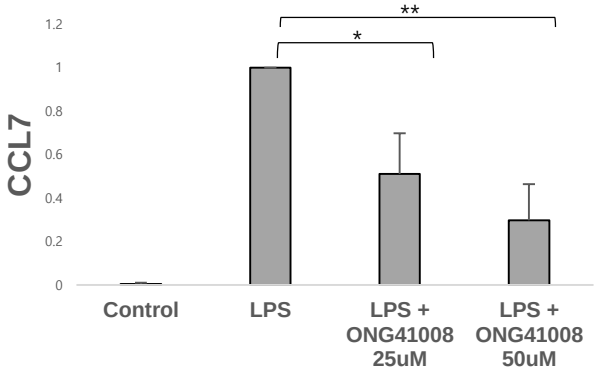

(D)

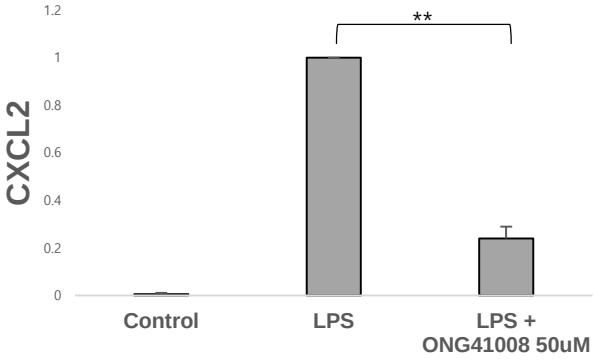

(E)

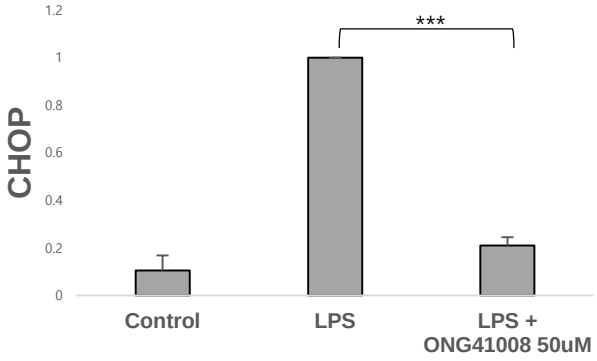

(F)

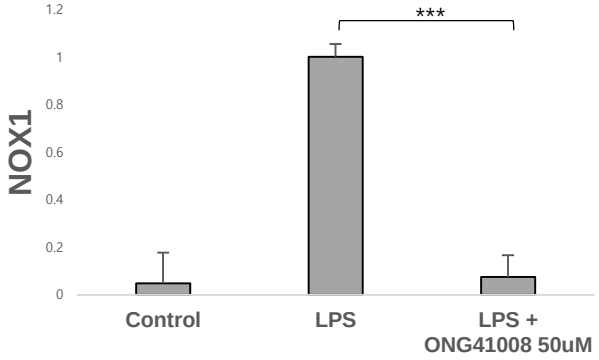

(G)

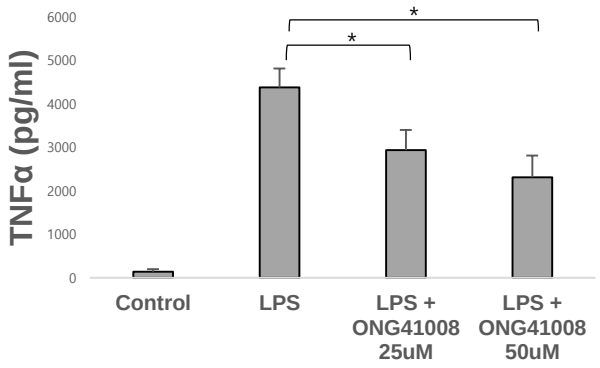

(H)

Figure 8

(A)

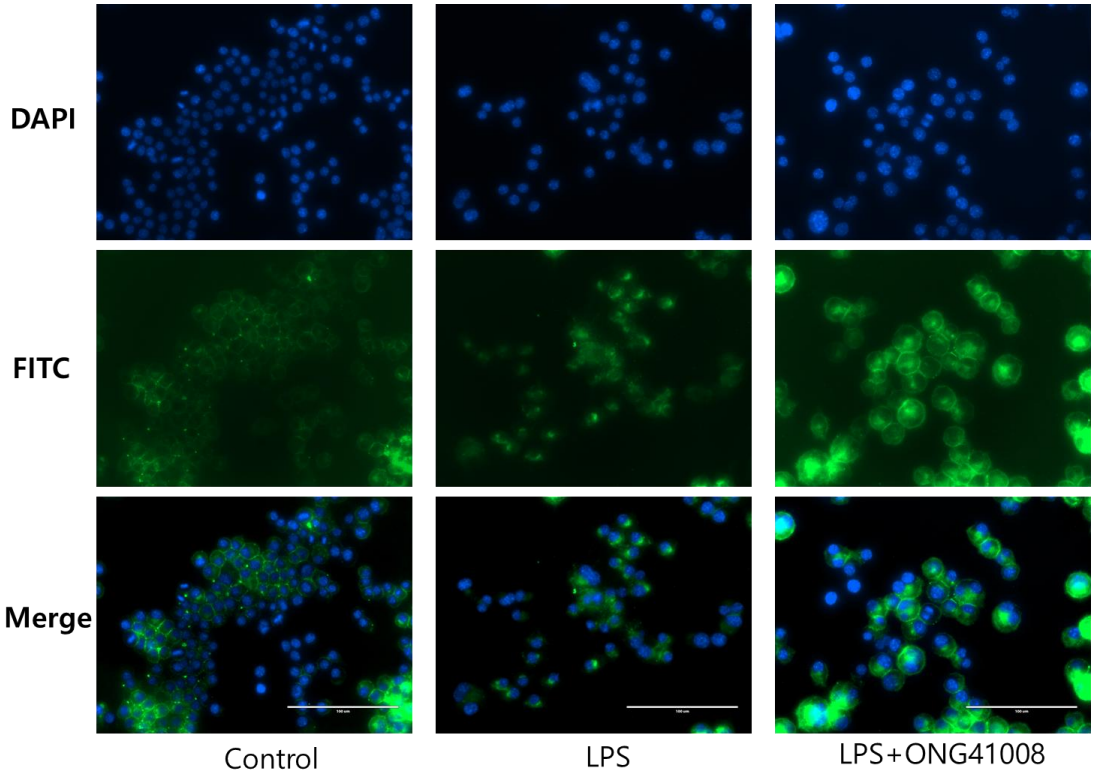
DAPI
FITC
Merge
Control
LPS
LPS+ONG41008

(B)

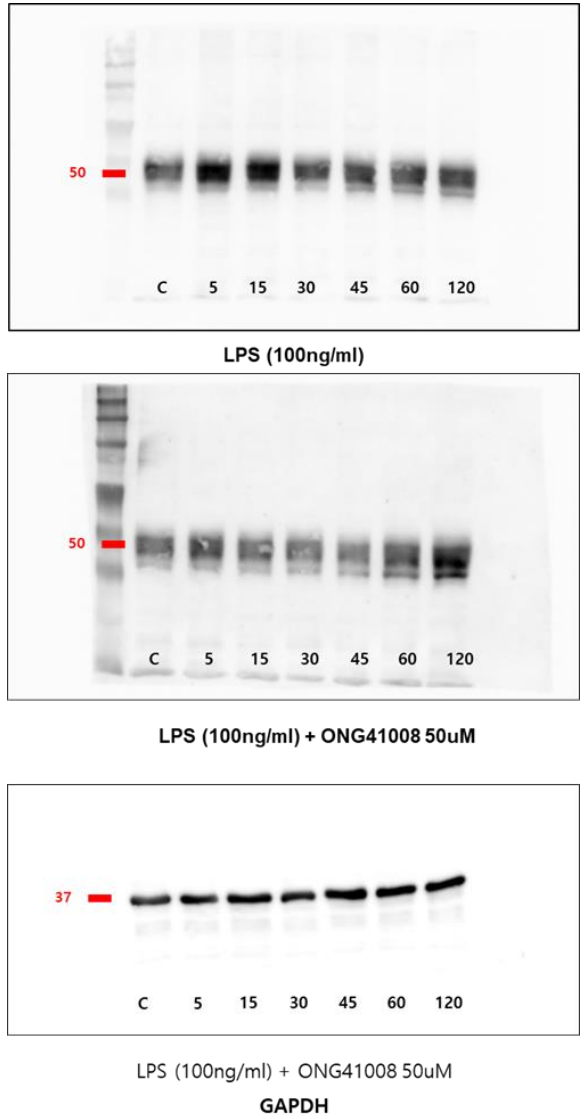
50
C 5 15 30 45 60 120
LPS (100ng/ml)
50
C 5 15 30 45 60 120
LPS (100ng/ml) + ONG41008 50uM
37
C 5 15 30 45 60 120
LPS (100ng/ml) + ONG41008 50uM
GAPDH

(C)

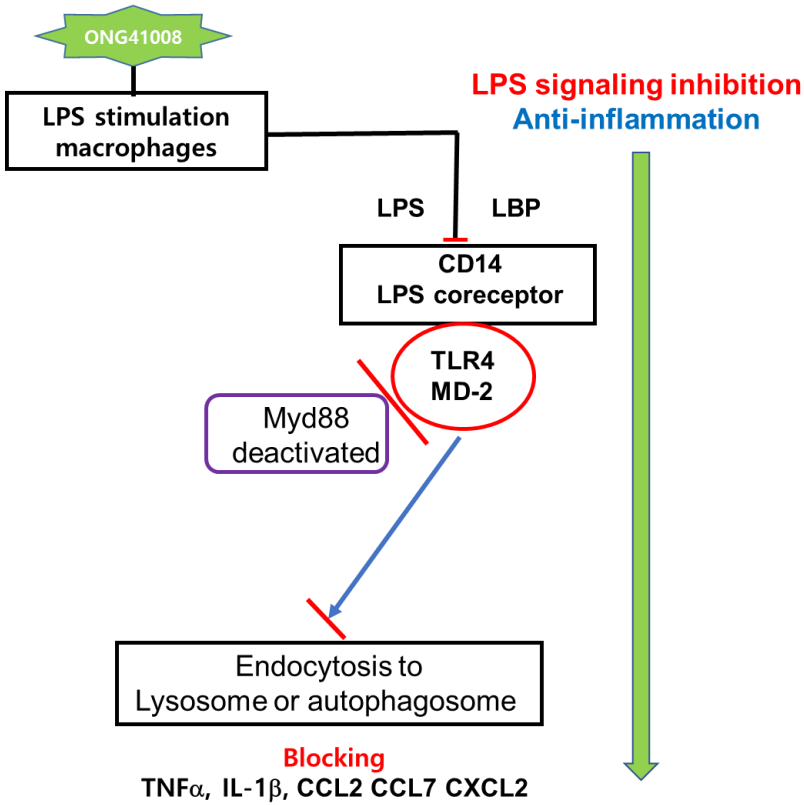
ONG41008
LPS stimulation macrophages
LPS signaling inhibition
Anti-inflammation
LPS
LBP
CD14
LPS coreceptor
TLR4
MD-2
Myd88 deactivated
Endocytosis to Lysosome or autophagosome
Blocking
TNFα, IL-1β, CCL2 CCL7 CXCL2

Figure 9